



**HAL**  
open science

# Oblique and streamwise vortex paths in a plane Couette flow using a RNL system

Frédéric Alizard

► **To cite this version:**

Frédéric Alizard. Oblique and streamwise vortex paths in a plane Couette flow using a RNL system. Comptes Rendus Mécanique, In press, pp.1-10. 10.5802/crmeca.55 . hal-03016962

**HAL Id: hal-03016962**

**<https://hal.science/hal-03016962>**

Submitted on 8 Dec 2020

**HAL** is a multi-disciplinary open access archive for the deposit and dissemination of scientific research documents, whether they are published or not. The documents may come from teaching and research institutions in France or abroad, or from public or private research centers.

L'archive ouverte pluridisciplinaire **HAL**, est destinée au dépôt et à la diffusion de documents scientifiques de niveau recherche, publiés ou non, émanant des établissements d'enseignement et de recherche français ou étrangers, des laboratoires publics ou privés.



---

# Oblique and streamwise vortex paths in a plane Couette flow using a RNL system

Frédéric Alizard<sup>a</sup>

<sup>a</sup> LMFA, UMR 5509, Univ Lyon, Université Claude Bernard Lyon 1, École Centrale de Lyon, INSA Lyon, CNRS, 43 boulevard du 11 novembre 1918, F-69100, VILLEURBANNE, France.

*E-mail:* frederic.alizard@univ-lyon1.fr, (F. Alizard).

## Abstract.

The present letter revisits the oblique wave and the streamwise vortex scenarios in a plane Couette flow using restricted nonlinear simulations where only a single Fourier mode for the perturbation is retained. It is shown that this restriction of the full dynamics gives a good approximation of the two subcritical paths. In particular, critical energy thresholds and edge states compare favorably with results obtained using direct numerical simulations by Duguet *et al.* (*Phys. Rev. E.*, 2010, 82, 026316).

**Keywords.** Shear flows, subcritical transition, reduced order model.

**Electronic supplementary material.** Supplementary material for this article is supplied as a separate archive available from the journal's website under article's URL or from the author.

This article is a draft (not yet accepted!)

## 1. Introduction

**Laminar/turbulent transition of wall-bounded shear flows is responsible for a dramatic increase in skin-friction drag for a wide variety of industrial applications. In that respect, the determination of which initial perturbation leads to transition is fundamental in order to design efficient control strategies.**

**The transition to turbulence often occurs even in the absence of an unstable linear mode associated with the laminar basic state. For this subcritical scenario, both the initial amplitude and spatial shape of the initial perturbation play prominent roles in triggering turbulence. To make progress in the understanding of the subcritical transition process, researchers have mainly focused on a small number of incompressible canonical flows.**

For instance, Kreiss *et al.* [1] and Reddy *et al.* [2] have first investigated the critical energy thresholds in both plane Couette flow (pCf) and channel flow for the streamwise vortex (SV) scenario and the oblique wave (OW) scenario using direct numerical simulations. For the SV scenario, the transition is initiated by streamwise vortices that generate streaks due to the lift-up effect [3]. When secondary perturbations are superimposed, the streak experiences a secondary instability and breaks down to turbulence. The second route to turbulence begins with a pair of

oblique waves that interact nonlinearly to create streamwise vortices. It leads to the formation of streaks that break down to turbulence due to secondary instability. For pCf, Reddy *et al.* [2] have found that the threshold energy density associated with the initial perturbation scales like  $Re^{-2.2}$  and  $Re^{-2.5}$ , where  $Re$  is the Reynolds number, for the streamwise vortex and the oblique wave scenarios, respectively. Later, Duguet *et al.* [4] have corrected the values given by Reddy *et al.* [2]. Especially, the authors found that the critical energy threshold scales like  $Re^{-2}$  for both OW and SV paths for the pCf. These scaling factors are consistent with the theoretical analysis of Chapman [5]. More recently, Karp *et al.* [6, 7] showed that the optimal set of parameters for transition in pCf is associated with initial disturbances which generate the strongest inflection point in the mean flow profile when nonlinearities come into play. In this vein, Cossu *et al.* [8] investigated the streak breakdown in a two-dimensional parameter space with respect to the amplitudes of the low-speed streak and its secondary perturbation. The authors showed that the transition is mainly associated with finite-amplitude disturbances that push the flow state along an unstable direction of the edge of chaos (Skufca [9]). In the same spirit, Duguet *et al.* [4] carried out optimizations to seek a minimal initial perturbation based on a linear combination of a finite number of linear optimal modes. When retaining three linear optimal modes, the authors found that the energy threshold of such a minimal perturbation is only 2% less than for a pair of symmetric oblique waves. For both SV and OW scenarios, they found that the trajectories closely approach two different steady states, so-called edge-states, with special symmetries.

Over the last decade, a lot of effort has been made in finding the weakest disturbance that can touch the edge of chaos. This perturbation is referred as the “minimal seed” and has the lowest energy on the edge. Using nonlinear optimisations, Monokrousos *et al.* [10], Rabin *et al.* [11] Duguet *et al.* [12] have identified a localised minimal disturbance in pCf. In particular, Duguet *et al.* [12] proposed a new scaling law for the minimal energy perturbation  $O(Re^{-2.7})$ , well below the energy threshold for the oblique wave scenario  $O(Re^{-2})$ . The temporal evolution of the minimal perturbation exhibits well-known linear mechanisms (Orr, lift-up, secondary streak instability) that the nonlinearity of the Navier-Stokes equations couples together [13]. Therefore, several attempts have been made to develop simplified models that are able to describe the main steps of the subcritical transition. A common aspect of all simplified models relies on the decomposition of the instantaneous flow fields into a streamwise averaged flow and a fluctuation. Nonlinearities are removed from the fluctuation equation, and a nonlinear feedback term is present in the streamwise-averaged part. For instance, using a single streamwise Fourier mode for the fluctuation and within the framework of the vortex-wave interaction (VWI) theory [14], Deguchi *et al.* and Deguchi [15, 16] established a Reynolds number scaling for transition in pCf:  $Re^{-2.5}$  close to the one found using DNS:  $Re^{-2.7}$ . One may recall that the VWI theory is consistent with the self-sustained process for asymptotically large Reynolds numbers [17, 18]. Biau & Bottaro [19] carried out nonlinear optimisations based on a similar decomposition, the so-called restricted nonlinear system [20] (RNL), to identify an optimal path to transition in a linearly stable duct flow. Similarly, Pralits *et al.* [21] showed that nonlinear optimisations based on a RNL system with a single streamwise Fourier mode and two spanwise Fourier modes is accurate to find an optimal path according to the oblique wave scenario. Nevertheless, none studies were devoted to clearly establish the ability of such RNL models to describe the OW and SV paths. In particular, are we able to recover the scaling laws found by Duguet *et al.* [4] using DNS, as suggested by the theoretical approach of Chapman [5] ? Especially, how the edge states associated with OW and SV paths are captured by RNL models ?

The scope of this paper is to shed some light onto these two points. For that purpose, the pCf case studied by Duguet *et al.* [4] will be investigated. A single Fourier mode for the fluctuation will be retained hereafter. The paper is then organised as follows. In section 2, we recall the equations of the RNL model. After presenting numerical methods, and the decomposition of the initial

perturbation as a finite number of linear optimal modes, the results are shown in section 3. A specific attention will be devoted to providing the Reynolds number scaling for both scenarios within a RNL framework, and to show the corresponding edge states. Finally, section 4 is devoted to conclusions and prospects.

## 2. Mathematical formulation

### 2.1. Restricted Non Linear model

We introduce the Cartesian coordinate system  $(x, y, z)$  and consider the plane Couette flow of an incompressible fluid with kinematic viscosity  $\nu$  between two parallel plates located at  $y = \pm h$ . The two plates move in opposite directions with velocity  $(\pm U_0, 0, 0)$ . The Reynolds number is defined as  $Re = U_0 h / \nu$ . We introduce the streamwise averaging operator over a streamwise distance  $L_x$  for any quantity  $\psi$ :

$$\bar{\psi}(y, z, t) = \frac{1}{L_x} \int_0^{L_x} \psi(x, y, z, t) dx. \quad (1)$$

The velocity disturbance to the Couette laminar solution ( $U_b = y, 0, 0$ ) is decomposed into its streamwise-averaged part  $\mathbf{U} = \bar{\mathbf{u}}$ , also called mean flow hereafter, and its fluctuation  $\tilde{\mathbf{u}}$ :

$$\mathbf{u}(x, y, z, t) = \mathbf{U}(y, z, t) + \tilde{\mathbf{u}}(x, y, z, t). \quad (2)$$

The components  $\mathbf{u} = (u, v, w)$  are streamwise, wall-normal and spanwise velocities, respectively. The pressure is similarly split into:  $p(x, y, z, t) = P(y, z, t) + \tilde{p}(x, y, z, t)$ .

Hereafter, we will consider a minimal RNL system where only a single streamwise component is retained. The fluctuations are thus expressed as:

$$\tilde{\mathbf{u}} = \hat{\mathbf{u}} e^{i\alpha x} + \hat{\mathbf{u}}^* e^{-i\alpha x},$$

where  $\alpha$  is the streamwise wave number ( $\alpha = 2\pi/L_x$ ), and  $*$  is used to denote the complex conjugate. The system of equations governing the streamwise-averaged flow reads:

$$V_y + W_z = 0,$$

$$U_t + V(U + U_b)_y + WU_z = Re^{-1}(U_{yy} + U_{zz}) - \partial_y(\hat{v}^* \hat{u} + \hat{v} \hat{u}^*) - \partial_z(\hat{w}^* \hat{u} + \hat{w} \hat{u}^*), \quad (3)$$

$$V_t + VV_y + WV_z = -P_y + Re^{-1}(V_{yy} + V_{zz}) - \partial_y(2\hat{v} \hat{v}^*) - \partial_z(\hat{w}^* \hat{v} + \hat{w} \hat{v}^*),$$

$$W_t + VW_y + WW_z = -P_z + Re^{-1}(W_{yy} + W_{zz}) - \partial_y(\hat{v}^* \hat{w} + \hat{v} \hat{w}^*) - \partial_z(2\hat{w}^* \hat{w}),$$

associated with homogeneous boundary conditions  $U = V = W = 0$  at the walls. The equations for the fluctuation, linearized around the mean flow, are:

$$i\alpha \hat{u} + \hat{v}_y + \hat{w}_z = 0,$$

$$\hat{u}_t + i\alpha(U + U_b)\hat{u} + \hat{v}(U + U_b)_y + V\hat{u}_y + \hat{w}U_z + W\hat{u}_z = -i\alpha\hat{p} + Re^{-1}(-\alpha^2\hat{u} + \hat{u}_{yy} + \hat{u}_{zz}), \quad (4)$$

$$\hat{v}_t + i\alpha(U + U_b)\hat{v} + \hat{v}V_y + V\hat{v}_y + \hat{w}V_z + W\hat{v}_z = -\hat{p}_y + Re^{-1}(-\alpha^2\hat{v} + \hat{v}_{yy} + \hat{v}_{zz}),$$

$$\hat{w}_t + i\alpha(U + U_b)\hat{w} + \hat{v}W_y + V\hat{w}_y + \hat{w}W_z + W\hat{w}_z = -\hat{p}_z + Re^{-1}(-\alpha^2\hat{w} + \hat{w}_{yy} + \hat{w}_{zz}),$$

together with  $\hat{u} = \hat{v} = \hat{w} = 0$  at the walls. The coupled system (3,4) is referenced as the RNL model.

## 2.2. Numerical methods and flow cases

For numerical integration of the RNL system, spectral approximations of the velocity fields are adopted, using Fourier expansions in both streamwise and spanwise directions and Chebyshev polynomials in the wall-normal direction. The numerical methods are described in Alizard [22] and the code has been validated in Alizard [23].

The flow cases investigated by [4, 12] are considered. The flow is simulated inside a computational box  $(L_x, L_y, L_z) = (4\pi, 2, 2\pi)$  with periodic boundary conditions in  $x$  and  $z$ . Six Reynolds numbers are investigated  $Re = 400, 750, 1500, 2000, 3000$  and  $3500$ . Accurate resolutions before dealiasing in  $z$  are achieved using  $(N_y, N_z) = (33, 48)$  for  $Re = 400$ ,  $(N_y, N_z) = (81, 64)$  for  $Re = 750$ ,  $(N_y, N_z) = (81, 96)$  for  $Re = 1500$  and  $2000$ ; and  $(N_y, N_z) = (81, 128)$  for  $Re = 3000, 3500$ . The  $3/2$  rule is used for dealiasing.

## 2.3. Initial perturbations

Following previous studies based on DNS [2, 4], the initial perturbation is constructed by summation of linear optimal modes. **A linear optimal mode is defined as the initial perturbation that maximizes kinetic energy gain over all times when the linearized Navier-Stokes operator is advanced forward in time [24].** For that:

$$\mathbf{U}(t=0) = \sum_i A_i \mathbf{U}_i, \text{ and } \tilde{\mathbf{u}}(t=0) = \sum_i a_i \tilde{\mathbf{u}}_i$$

where each mode  $\mathbf{U}_i$  corresponds to an optimal mode with  $\alpha = 0$  and different harmonics in  $z$ . Modes  $\tilde{\mathbf{u}}_i$  correspond to optimal modes with  $\alpha = 0.5$  ( $L_x = 4\pi$ ) and different harmonics in  $z$ . The complex amplitudes of the different modes are noted  $A_i$  and  $a_i$ .

The kinetic energy threshold for transition is determined using a bisection algorithm. In that respect, we introduce the scalar function as in Duguet *et al.* [4]:

$$E_c : (\Re(A_1), \Im(A_1), \Re(a_1), \Im(a_1), \dots, \Re(A_N), \Im(A_N), \Re(a_M), \Im(a_M)) \rightarrow E_c$$

where  $N$  modes and  $M$  modes are considered for the streamwise averaged quantity and fluctuation, respectively.

Hereafter, Fourier modes corresponding to the wavevector components  $(n\alpha, m\beta)$  with  $(\alpha, \beta) = (2\pi/L_x, 2\pi/L_z)$  are labelled by  $(m, n)$ . In the present study, we will restrict our analysis to two different cases. For the oblique path, a pair of oblique waves with equal amplitude  $(1, \pm 1)$  is chosen as initial perturbation. For the latter, the only unknown is the amplitude of the perturbation that is fixed through the bisection algorithm. For the SV scenario, the initial subspace for the perturbation is reduced to two optimal modes  $(0, 2)$  and  $(1, 2)$ . Considering the symmetries in  $x$  and  $z$ , the amplitude coefficients  $\Re(A_1), \Im(A_1), \Re(a_1), \Im(a_1), \dots$  are reduced to 1 parameter noted  $\lambda$ . **The integrated kinetic energies for the perturbation and the mean flow are noted  $E_p(t)$  and  $E_M(t)$ , respectively. They are defined as:**

$$E_p(t) = \frac{1}{L_y L_z} \int_{L_y L_z} \hat{\mathbf{u}}(y, z, t) \cdot \hat{\mathbf{u}}^*(y, z, t) dy dz, \quad E_M(t) = \frac{1}{2L_y L_z} \int_{L_y L_z} \mathbf{U}(y, z, t) \cdot \mathbf{U}(y, z, t) dy dz.$$

Without loss of generality,  $\lambda$  is fixed to  $E_p(t=0)/E_M(t=0)$ . In this case, the expression of  $E_c$  is reduced to  $E_c(\lambda)$ . In Duguet *et al.* [4], the minimisation of  $E_c$  is carried out using a Newton algorithm. Here, we will investigate the distribution of  $E_c$  with  $\lambda$ . The stopping criterion of the bisection algorithm is fixed to  $r = |(E_c^{i+1} - E_c^i)|/E_c^i < 10^{-4}$  for a given iteration  $i$ . The critical energy threshold includes both contributions **for the SV scenario ( $E_M(t=0) + E_p(t=0)$ ) and only the kinetic energy of the fluctuation for the OW case ( $E_p(t=0)$ ).**

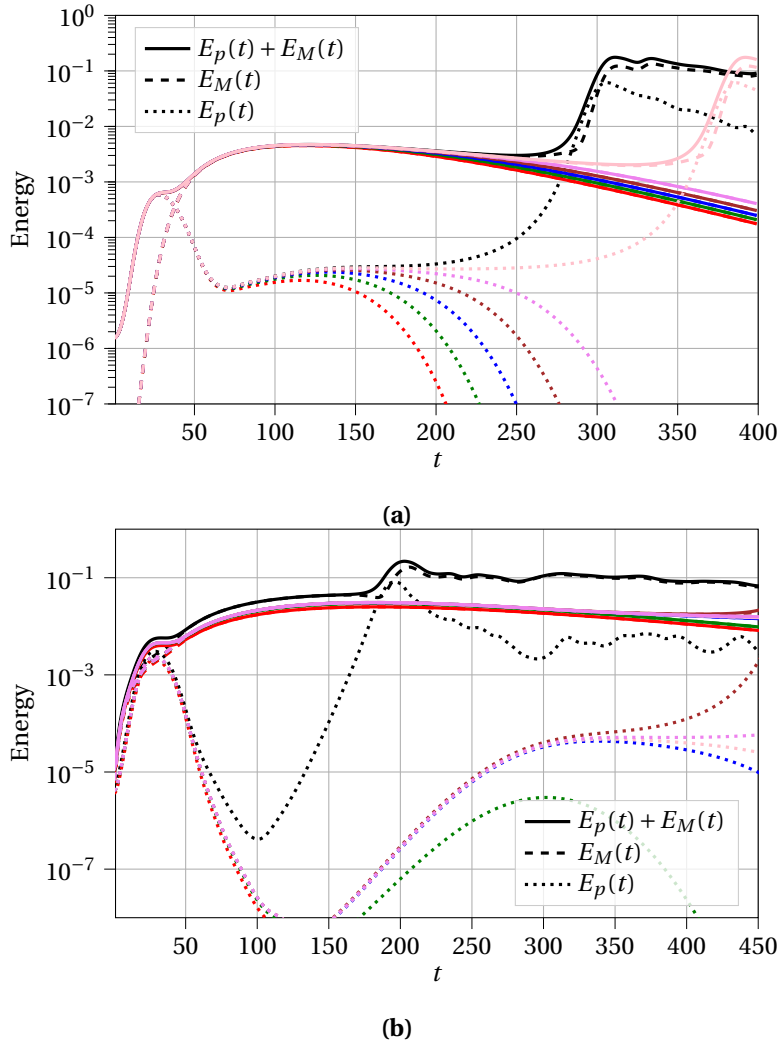


**Figure 1.** Illustration of the bisection algorithm for  $Re = 1500$ . Integrated kinetic energy of the perturbation velocity versus time when varying the initial amplitude. (a) Pure oblique wave scenario. (b) Streamwise vortex scenario. **For case (b), the amplitude  $\lambda$  is associated with the minimum of  $E_c(\lambda)$ .**

### 3. Results

#### 3.1. Kinetic energy thresholds

The results of RNL simulations corresponding to the pure OW and SV scenarios are now presented in parallel. In figure 1, we show the integrated kinetic energy of the perturbation (both fluctuation and mean flow contributions) as a function of time when varying the initial amplitude. For illustration purpose, the Reynolds number is here fixed to  $Re = 1500$ . The figure shows that for the two cases, the bisection algorithm converges to an almost steady state where  $E_p(t)$  and  $E_M(t)$  reach a plateau before breakdown. **At the convergence, the critical energy threshold is  $E_c = E_M(t=0) + E_p(t=0)$ .** One may also notice that for an initial kinetic energy slightly above

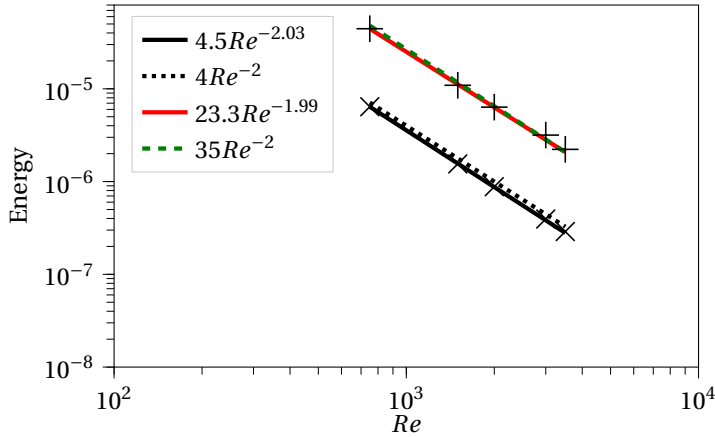


**Figure 2.** Energy threshold versus the Reynolds number  $Re$  for  $Re = 750, 1500, 2000, 3000$  and  $3500$  obtained by using RNL simulations (symbols). The fitted curves for oblique waves and streamwise vortex scenarios using RNL simulations (full lines) are compared with values provided by [4] using fully nonlinear simulations (dashed lines). The Re-scaling law for the OW scenario is  $4.5Re^{-2.03}$ . For the SV scenario, the Re-scaling law is  $23.3Re^{-1.99}$ .

$E_c$ , the integration forward in time of the initial perturbation leads to a self-sustained state for long times.

The variations of threshold energy  $E_c$  with the Reynolds number are shown in figure 2 for the pure oblique wave scenario and the streamwise vortex scenario. The minimization of  $E_c$  is used to fix  $\lambda$  for the SV case. The figure 2 shows that the exponent predicted by the RNL model is in perfect agreement with the full DNS for both scenarios (*i.e.*  $-2$ ). In addition, kinetic energy thresholds obtained using the RNL system are almost superimposed with those found using the full nonlinear system. This finding is in agreement with the theoretical development of Chapman [5].

To better appreciate the relevance of the strong restriction associated with the RNL model in describing OW path, the variation of the threshold kinetic energy with the streamwise extent is shown in figure 3 for  $Re = 400$ . Results provided by Duguet *et al.* [4] are also shown. **We recall that for this case, we consider  $(N_y, N_z) = (33, 48)$ .** The oblique wave structure leading to transition with the lowest energy density has a streamwise wavelength  $L_x \approx 6\pi$  when considering the RNL system. The full DNS gives  $L_x \approx 5.5\pi$  [4]. This corresponds to an angle with respect to the streamwise direction of  $20^\circ$  for the DNS and  $18.5^\circ$  for the RNL model. It illustrates that the RNL model is quite accurate to provide the direction of the most efficient oblique wave. Furthermore, the kinetic energy threshold for the optimal wavelength obtained using RNL simulations ( $2.09 \times 10^{-5}$ ) is also quite close to the one obtained by DNS ( $2.92 \times 10^{-5}$ ).

### 3.2. Edge states

In the previous section, it was shown that for both OW and SV paths, when the initial kinetic energy is fixed to  $E_c$ , the trajectory passes close to a steady state. It is suggested that such a state corresponds to an edge state. To better confirm this assumption, we consider hereafter the same flow case as Duguet *et al.* [4] ( $Re = 400$ ). To find the corresponding edge state, the stopping criterion associated with the bisection algorithm is fixed to  $r = 10^{-6}$ . The edge state found using a pair of oblique waves with equal amplitudes is shown in figure 4. This steady state exhibits the

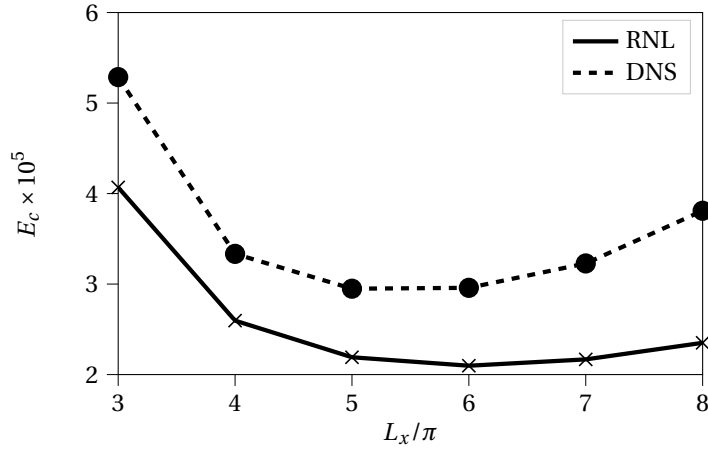


**Figure 3.**  $Re = 400$ . Threshold kinetic energy for the transition initiated by a pair of symmetric oblique waves as a function of the streamwise length. DNS results are extracted from Duguet *et al.* [4].

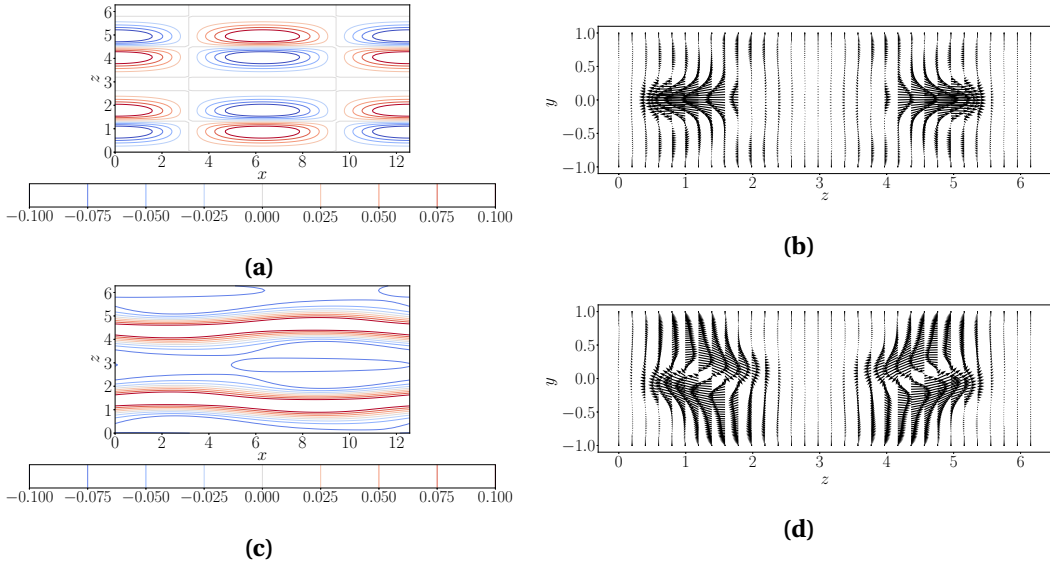


**Figure 4.**  $Re = 400$ . Edge state  $E1$  approached by an initial perturbation composed of a pair of symmetric oblique waves. Isocontours of the streamwise velocity fields extracted at the planes  $y = 0$  (a) and  $y = 0.4$  (c). Vectors for the cross-stream components extracted at the planes  $x = 3.2$  (b) and  $x = 0.4$  (d).

same feature that the state  $E1$  found using full DNS by Duguet *et al.* [4]. In particular,  $E1$  displays low-speed streaks with a varicose structure in both simulations. Both states lie in the same spatial symmetry subspace associated with the following transformations (the notations of Duguet *et al.* [4] are used):

$$\begin{aligned}
 g_1 : [u, v, w](x, y, z) &= [u, v, w](x + L_x/2, y, z + L_z/2), \\
 g_2 : [u, v, w](x, y, z) &= [u, v, -w](x, y, -z), \\
 g_3 : [u, v, w](x, y, z) &= [-u, -v, w](-x, -y, z)
 \end{aligned}$$

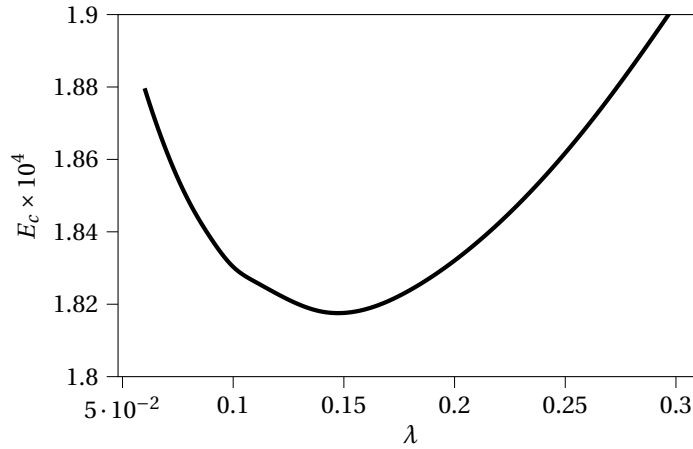


**Figure 5.**  $Re = 400$ . Threshold kinetic energy for transition initiated by modes (0,2) and (1,2) as a function of  $\lambda$ .

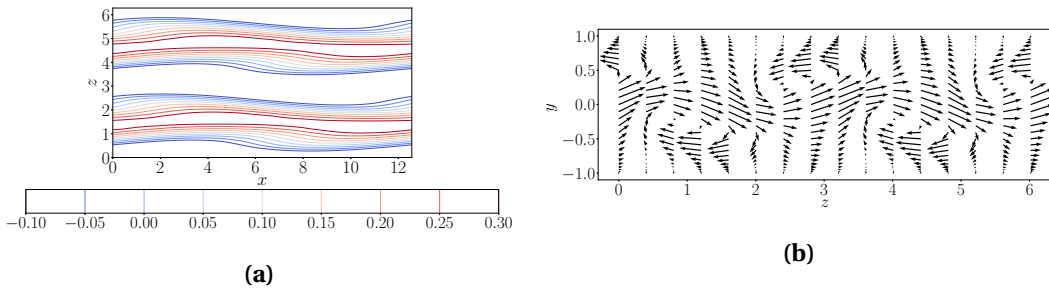


**Figure 6.**  $Re = 400$ . Edge state for initial perturbation associated with modes (0,2) and (1,2) for  $\lambda = 0.14$ . Isocontours of the streamwise velocity fields extracted at the planes  $y = 0$  (a) and vectors for the cross-stream components extracted at the plane  $x = 3.2$  (b).

as well as any combinations of those symmetries.

For the streamwise vortex scenario, the initial perturbation is driven by modes (0,2) and (1,2). In figure 5, the distribution of the critical initial kinetic energy as a function of  $\lambda$  is displayed. The figure shows that an optimal value of  $\lambda$  is around 0.14. For the full DNS, Duguet *et al.* [4] have found  $\lambda = 0.0965$  which is quite close to the one provided by the RNL approximation. Furthermore, the figure also shows that the improvement in terms of critical energy is weak (only 5% for the range of  $\lambda$  that is investigated). This remark is consistent with the observations of Duguet *et al.* [4]. The edge state is shown in figure 6. The latter shares strong similarities with the state referenced as  $E2$  in [4]. Especially,  $E2$  exhibits a sinuous motion of a pair of low- and high-speed streaks and have the following symmetries (the notations of Duguet *et al.* [4] are used):

$$\begin{aligned} s_1 : [u, v, w](x, y, z) &= [u, v, -w](x + L_x/2, y, -z), \\ s_2 : [u, v, w](x, y, z) &= [-u, -v, w](-x, -y, -z + L_z/2), \\ s_3 : [u, v, w](x, y, z) &= [-u, -v, -w](-x + L_x/2, -y, -z + L_z/2) \end{aligned}$$

Hence, the phase space trajectories are seen to be also well reproduced for both OW and SV scenarios.

## 4. Conclusions

This study revisits the oblique wave and streamwise vortex scenarios for subcritical transition in a plane Couette flow within a restricted nonlinear framework. It is shown that the strong restriction of the full dynamics associated with the RNL system using a single streamwise Fourier mode for the perturbation allows to well describe both subcritical paths. Especially, the critical energy threshold is seen to scale as  $Re^{-2}$  for the two subcritical scenarios, in agreement with the theoretical study provided by Chapman [5] and direct numerical simulations carried out by Duguet *et al.* [4]. More interestingly, the distributions of the critical energy thresholds with the Reynolds number are almost superimposed for both simulations. Furthermore, the corresponding phase space trajectories are also well described by the RNL approximation for the two scenarios. In particular, the edge states found by Duguet *et al.* [4] are well recovered using the simplified set of equations.

We believe that such a confirmation is a preliminary step to approximate the minimal seed in parallel shear flows using RNL models that are classically found using extensive nonlinear optimisations based on full DNS [13, 25]. In such a perspective, the optimisation procedure derived by Biau & Bottaro [19] could be an attractive prospect. This work is currently in progress. **In particular, since the RNL system prevents any streamwise localisation, this analysis should also indicate which role plays spanwise localisation in the Re-scaling law found by Duguet *et al.* [12].**

It should also be interesting to carry out optimisations as those done by Duguet *et al.* [4] using a larger subspace for the linear optimal modes basis and including the target times as an optimisation parameter. While within a DNS framework, such optimisations require a huge numerical effort, this could be more easily achieved using the RNL simplification. In that respect, it would be of interest to evaluate the possibility of spanwise localisation for the initial perturbation when increasing the number of linear optimal modes.

**Finally, since subcritical paths leading to turbulence (OW and SV) are well described within the RNL framework, one may suggest to use the RNL system to design controllers which can be applied on the full nonlinear dynamics.**

This work was granted access to the HPC resources of the FLMSN, “Fédération Lyonnaise de Modélisation et Sciences Numériques”, partner of EQUIPEX EQUIP@MESO.

The numerical codes and data that have been used for this study can be available from the corresponding author upon request.

## References

- [1] G. Kreiss, A. Lundbladh, D. Henningson, “Bounds for threshold amplitudes in subcritical shear flows”, *J. Fluid Mech.* **270** (1994), p. 175-198.
- [2] S. Reddy, P. Schmid, J. Baggett, D. S. Henningson, “On stability of streamwise streaks and transition thresholds in plane channel flows”, *J. Fluid Mech.* **365** (1998), p. 269-303.
- [3] M. Landhal, “A note on an algebraic instability of inviscid parallel shear flow.”, *J. Fluid Mech.* **98** (1980), p. 243-251.
- [4] Y. Duguet, L. Brandt, B. Larson, “Towards minimal perturbations in transitional plane Couette flow”, *Phys. Rev. E* **82** (2010), p. 026316.
- [5] S. Chapman, “Subcritical transition in channel flows”, *J. Fluid Mech.* **451** (2002), p. 35-97.
- [6] M. Karp, J. Cohen, “Tracking stages of transition in Couette flow analytically”, *J. Fluid Mech.* **748** (2014), p. 896-931.
- [7] M. Karp, J. Cohen, “On the secondary instabilities of transient growth in Couette flow”, *J. Fluid Mech.* **813** (2017), p. 528-557.
- [8] C. Cossu, L. Brandt, S. Bagheri, D. Henningson, “Secondary threshold amplitudes for sinuous streak breakdown”, *Physics of Fluids* **23** (2011), p. 074103.

- [9] J. D. Skufca, J. A. Yorke, B. Eckhardt, “Edge of chaos in a parallel shear flow”, *Phys. Rev. Lett.* **96** (2006), p. 174101.
- [10] A. Monokrousos, A. Bottaro, L. Brandt, A. Di Vita, D. S. Henningson, “Nonequilibrium Thermodynamics and the optimal path to turbulence in shear flows”, *Phys. Rev. Lett.* **106** (2011), p. 134502.
- [11] S. M. E. Rabin, C. P. Caulfield, R. Kerswell, “Triggering turbulence efficiently in plane Couette flow”, *J. Fluid Mech.* **712** (2012), p. 244-272.
- [12] Y. Duguet, A. Monokrousos, L. Brandt, “Minimal transition thresholds in plane Couette flow”, *Physics of Fluids* **25** (2013), p. 084103.
- [13] R. R. Kerswell, “Nonlinear Nonmodal Stability Theory”, *Annual Review of Fluid Mechanics* **50** (2018), p. 319-345.
- [14] P. Hall, F. Smith, “On strongly nonlinear vortex/wave interactions in boundary-layer transition”, *J. Fluid Mech.* **227** (1991), p. 641-666.
- [15] K. Deguchi, P. Hall, A. Watson, “The emergence of localized vortex-wave interaction states in plane Couette flow.”, *J. Fluid Mech.* **721** (2013), p. 58-85.
- [16] K. Deguchi, “Self-sustained states at Kolmogorov microscale”, *J. Fluid Mech.* **781** (2015), p. R6.
- [17] J. M. Hamilton, J. Kim, F. Waleffe, “Regeneration mechanisms of near-wall turbulence structures”, *J. Fluid Mech.* **287** (1995), p. 317-348.
- [18] J. Wang, J. Gibson, F. Waleffe, “Lower Branch Coherent States in Shear Flows: Transition and Control”, *Phys. Rev. Lett.* **98** (2007), p. 204501.
- [19] D. Biau, A. Bottaro, “An optimal path to transition in a duct”, *Phil. Transact. Royal Soc.* **367** (2009), p. 529-544.
- [20] B. F. Farrell, P. J. Ioannou, “Dynamics of streamwise rolls and streaks in turbulent wall-bounded shear flow”, *J. Fluid Mech.* **708** (2012), p. 149-196.
- [21] J. O. Pralits, A. Bottaro, S. Cherubini, “Weakly nonlinear optimal perturbations.”, *J. Fluid Mech.* **785** (2015), p. 135-151.
- [22] F. Alizard, “Linear stability of optimal streaks in the log-layer of turbulent channel flows”, *Physics of Fluids* **27** (2015), p. 105103.
- [23] F. Alizard, “Invariant solutions in a channel flow using a minimal restricted nonlinear model”, *C.R. Mécanique* **345** (2017), p. 117-124.
- [24] P. Schmid, D. Henningson, *Stability and Transition in Shear Flows*, Applied Mathematical Sciences 142, Springer, 2001.
- [25] C. Pringle, R. Kerswell, “Using nonlinear transient growth to construct the minimal seed for shear flow turbulence”, *Phys. Rev. Lett.* **105** (2010), p. 154502.